Research Article

3D-printed micro-axicon enables extended depth-of-focus intravascular optical coherence tomography *in vivo*

Pavel Ruchka[a], Alok Kushwaha,[b,c] Jessica A. Marathe,[d,e,f] Lei Xiang,[b,c] Rouyan Chen,[b,c,f] Rodney Kirk,[c,d]
Joanne T. M. Tan,[d,f] Christina A. Bursill,[d,f] Johan Verjans,[d,e,f] Simon Thiele,[g] Robert Fitridge,[d,h]
Robert A. McLaughlin,[c,d] Peter J. Psaltis,[d,e,f] Harald Giessen,[a] and Jiawen Li[b,c,f,*]

aUniversity of Stuttgart, 4th Physics Institute and Research Center SCoPE, Stuttgart, Germany
bUniversity of Adelaide, School of Electrical and Mechanical Engineering, Adelaide, South Australia, Australia
cUniversity of Adelaide, Institute for Photonics and Advanced Sensing, Adelaide, South Australia, Australia
dUniversity of Adelaide, Faculty of Health and Medical Sciences, Adelaide, South Australia, Australia
eCentral Adelaide Local Health Network, Department of Cardiology, Adelaide, South Australia, Australia
fSouth Australian Health and Medical Research Institute (SAHMRI), Lifelong Health Theme, Adelaide, South Australia, Australia
gPrintoptix GmbH, Stuttgart, Germany
hCentral Adelaide Local Health Network, Vascular and Endovascular Service, Adelaide, South Australia, Australia

Abstract. A fundamental challenge in endoscopy is how to fabricate a small fiber-optic probe that can achieve comparable function to devices with large, complicated optics. To achieve high resolution over an extended depth of focus (DOF), the application of needle-like beams has been proposed. However, existing methods for miniaturized needle-beam designs fail to adequately correct astigmatism and other monochromatic aberrations, limiting the resolution of at least one axis. Here, we describe an approach to realize freeform beam-shaping endoscopic probes via two-photon polymerization three-dimensional (3D) printing. We present a design achieving $<8\ \mu m$ lateral resolution with a DOF of $\sim 800\ \mu m$. The probe has a diameter of $<260\ \mu m$ (without the torque coil and catheters) and is fabricated using a single printing step directly on the optical fiber. The probe was successfully utilized for intravascular imaging in living diabetic swine at multiple time points, as well as human atherosclerotic plaques *ex vivo*. To the best of our knowledge, this is the first report of a 3D-printed micro-optic for *in vivo* imaging of the coronary arteries. These results are a substantial step to enable the clinical adoption of both 3D-printed micro-optics and beam-tailoring devices.

Keywords: optical coherence tomography; two-photon polymerization three-dimensional printing; intravascular imaging; beam shaping; Bessel beam.

Received Oct. 1, 2024; revised manuscript received Dec. 22, 2024; accepted for publication Jan. 20, 2025; published online Mar. 3, 2025.

1 Introduction

Life-threatening diseases, such as coronary artery and cerebrovascular diseases, are often related to the presence of atherosclerotic plaques. Optical coherence tomography (OCT) is a promising technique for *in vivo* assessment of atherosclerotic plaques. In particular, intravascular OCT, which can characterize high-risk atherosclerotic plaques, is commonly used in coronary

arteries to help diagnose high-risk plaques and potentially guide treatment to prevent heart attacks.[1,2]

Intravascular imaging inside small- to moderate-sized arteries, such as coronaries, enforces extremely limiting restrictions on fiber-optic OCT probes. The focusing optics of the OCT probe must be small enough to image safely inside a narrow blood vessel, which limits the sophistication of the optical design. The probe is encased within a protective catheter, which also introduces optical aberrations, such as astigmatism.[3,4] Although current commercially available probes have demonstrated

clinical value, they fail to exploit the cellular-resolution diagnostic potential of OCT.[5] A key challenge is to enable high-resolution intravascular imaging over an extended depth of focus (DOF).[6]

Needle beams (also called Bessel beams) are one approach designed to maintain high resolution over a greater depth than is possible with conventional Gaussian beams. Needle beams are widely used in advanced microscopy, including OCT,[5–8] light-sheet microscopy,[9,10] multiphoton microscopy,[11,12] and photoacoustic microscopy,[13,14] due to their extended DOF with a small lateral extension of the beam. Various approaches have been proposed to achieve needle-shaped beams for extended DOF in OCT endoscopes, including axicon lenses fabricated by molding a fiber,[15] spatial filters[16,17] or annual apodization,[5,18] phase masks,[7] tailored chromatic dispersion,[4] and multimode fibers,[6,19] as discussed in Table S1 in the Supplementary Material. However, until now, it has been unfeasible to fabricate a needle-beam fiber-optic device without astigmatism for imaging of a blood vessel.[7,20–22]

Two-photon polymerization three-dimensional (3D) printing is a high-resolution additive manufacturing process that can fabricate freeform optical structures at the micrometer scale. Preliminary work has demonstrated the potential to correct for astigmatism[3] and fabricate more complex, multipart optical designs.[23]

In this study, we describe the development of a high-resolution, 3D-printed fiber-optic endoscopic probe that utilizes a side-facing micro-axicon lens to acquire 3D images inside the blood vessels. This lens design also corrects for the astigmatism of the protective intracoronary catheter. We characterize the probe, demonstrating a clear superiority in imaging resolution over a standard gradient index (GRIN) fiber design and demonstrate its use in both *ex vivo* imaging of atherosclerotic plaques in a human artery and longitudinally *in vivo* imaging in a diabetic porcine model of coronary artery disease. The size of the porcine thorax and the location of atherosclerotic lesions, particularly in the coronaries, closely resemble the human anatomy. Porcine models are commonly used before the first-in-human study. This porcine study forms an important stage in the path to clinical adoption of 3D-printed micro-optics.

2 Materials and Methods

2.1 Design of Freeform Needle Beam Endoscopic Probe

Figure 1(a) depicts the general concept of the 3D-printed needle beam fiber-optic probe for OCT. This design is optimized for the use case of operating the probe for *in vivo* imaging inside coronary arteries, i.e., vessels with a diameter between 2 and 3 mm. Figure 1(b) presents the sketch of the optical design. The probe was designed using commercial ray-tracing software, Zemax OpticStudio (Ansys, Inc., Canonsburg, Pennsylvania, United States). The goal of the probe design is to enable high-resolution OCT imaging over an extended DOF while maintaining a small footprint for safe intracoronary imaging.

In cardiology, catheter sheaths are commonly used to safeguard delicate endoscopic probes from contamination and mechanical damage, which poses significant challenges for the design of the beam-transforming optics. This is because catheter sheaths introduce strong astigmatism and therefore

elongate the beams in one direction, leading to low resolution. In our fiber-optic probe, there are two tubes: an inner protective tube and an intracoronary catheter sheath. The inner tube protects the 3D-printed lens as it is inserted into the intracoronary catheter sheath. The intracoronary catheter sheath is then used to enable the placement of the fiber-optic probe within the coronary artery under fluoroscopic and angiographic guidance.[24] Key aspects of the resulting 3D-printed lens design include the mechanism used to redirect the light to achieve side-viewing toward the vessel walls, compensation for astigmatism inherent in this setup (i.e., the inner protective tube and the intracoronary catheter sheath), and achieving high lateral resolution over an extended imaging range.

Redirecting the light beam toward the vessel walls is achieved by integrating a reflective surface into the optical design. There are multiple potential approaches to enable this. Recently, a dual-axis catadioptric system was proposed where the mirror to deflect the beam sideways was manufactured by vapor deposition of a gold layer.[25] However, this requires additional manufacturing steps, increasing fabrication time and complexity. Our design avoids the need to include a metallic layer; instead, we use total internal reflection (TIR) at the air–photoresist interface by ensuring that the incident angle of the light upon the surface is greater than the critical angle of 41 deg. The reflected light beam propagates at an angle of 80 deg to the optical axis of the final lens. The output surface of the lens is an axicon with aspheric terms that compensate for irregularities in intensity distribution along the propagation axis. To obtain the axicon surface, we choose an odd asphere surface type in Zemax OpticStudio and set the polynomial orders 1 to 5 as variables. The merit function for the optimization is defined to obtain the best radial spot size over the desired DOF. The size of the 3D-printed lens is chosen so that the axicon tip sits extremely close to the inner surface of the protective tube (inner diameter ID: 370 μm), minimizing the path length in the air to the vessel walls. This 3D-printed micro-axicon forms a needle beam, which then propagates through both catheters at an angle of 10 deg in the meridional plane.

Second, we created a biconical surface, which allows it to compensate for the strong astigmatism from two tubes. In our case, the biconical surface is flat in one plane and features a negative radius of curvature to compensate positive radii of the protective tube and catheter sheath. In essence, we compensate for the astigmatic tubes with a 3D-printed astigmatic freeform. Opting for a simpler biconic surface rather than a complete freeform surface provides a more uniform reflection over a wider range of angles and allows easier optimization of the TIR surface.[26]

Finally, after passing through both tubes, the light beam propagates through 1 mm of the blood-like medium before reaching the vessel wall. Figures 1(c) and 1(d) illustrate the design by microscopic images. The needle beam starts at the apex of the micro-axicon lens. Note that the starting point of the needle-beam and its intensity distribution can be adjusted by tuning the aspheric terms and by controlling the sharpness of the axicon tip.

2.2 Fabrication of the 3D-Printed Needle Beam Endoscopic Probe

Before printing, we prepared the fiber by splicing a no-core fiber (FG125LA, Thorlabs, Newton, New Jersey, United States) to a single-mode fiber (SMF28, Thorlabs, Newton, New Jersey,
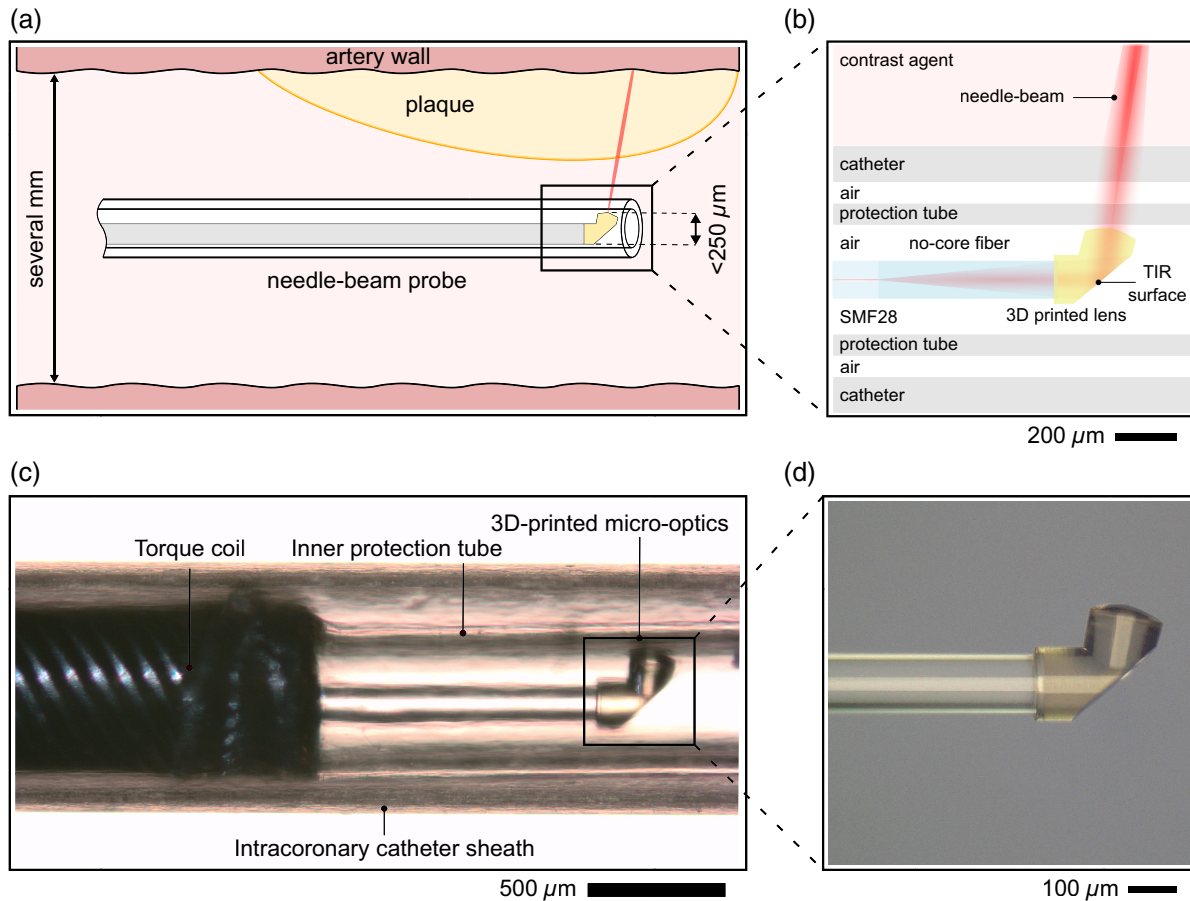
Fig. 1 3D-printed needle-beam endoscopic probe design. (a) Sketch of the optical design of the 3D-printed needle-beam probe. Here, we omit the mechanical parts, which are irrelevant from the optical standpoint. (b) Close-up schematic to highlight the distal end of the needle-beam probe. The laser beam at 1310 nm comes from SMF28 fiber and gets expanded in a spliced piece of no-core fiber. The lens is 3D-printed directly onto the cleaved facet of the no-core fiber in one step. The 3D-printed biconic TIR surface reflects the beam under an 80-deg angle to the optical axis of the fiber and precompensates the astigmatism arising from the protection tube and the catheter. After reflection at the TIR surface, the Gaussian laser beam is shaped to the needle beam by an axicon exit surface. (c) Optical microscope image of the fully assembled needle-beam probe at its distal end. (d) Zoom in to the 3D-printed micro-axicon micro-optics.

United States) using a fiber-processing machine (Vytran GPX3800, Vytran, Exeter, United Kingdom). With the same machine, we cleaved the no-core fiber to the length of 600 μm. After cleaving, we silanized the fiber probes for at least 2 h using a solution of 30 mL of ethanol and 150 μL of 3-(trimethoxysilyl)propyl methacrylate to increase the adhesion between the photopolymer and the fiber facet.

The axicon lens with the TIR surface was printed after the silanization directly onto the fiber facet using Nanoscribe Photonic Professional GT (Nanoscribe GmbH, Eggenstein-Leopoldshafen, Germany). We used the commercially available photopolymer IP-S (Nanoscribe GmbH, Eggenstein-Leopoldshafen, Germany) to print the structure as this photopolymer provides the smoothest surface, which is crucial to achieve the desired TIR with a reasonable budget for the printing imperfections. We used a slicing distance of 0.1 μm and a hatching distance of 0.15 μm with a laser power of 36 mW and a scanning speed of 50 mm/s. The needle-beam probe was printed within 3.5 h. For the development, we used a commercially available

developer mr-Dev600 (micro resist technology GmbH, Berlin, Germany) for 15 min and isopropanol for 3 min to rinse the printed structure. Afterward, we proceeded with 5-min UV curing with a deep-UV lamp (DYMAX BlueWave 50, Torrington, United States) to ensure that the structure was fully polymerized and the refractive index was homogeneous.

The 3D-printed needle-beam fiber probe was placed inside a torque coil (ID of 0.25 mm and outer diameter of 0.5 mm, Asahi Intecc Co., Seto, Japan). The distal end of the fiber probe was protected by the inner tube (Zeus, Inc., Orangeburg, United States). The protected fiber probe was then inserted into a commercially available intracoronary catheter sheath (Dragonfly, Abbott, Chicago, Illinois, United States) for *in vivo* porcine experiments. Before each *in vivo* experiment, we sterilized the imaging catheters to be used, in which the 3D-printed needle-beam probes sit, using ethylene oxide (ETO), a typical way to sterilize medical packaging and device lumens. As a long aeration time is needed to remove ETO residue, imaging catheters were given to the animal tech team at least 24 h

before the imaging procedure to ensure sufficient time for sterilization and aeration.

2.3 Back-End Imaging System

The 3D-printed needle-beam endoscopic probe was connected to an OCT imaging system. This system used the light source and detector of a commercially available OCT system (with a −5-dB bandwidth of the light source ranging from 1185 to 1415 nm and a central wavelength at 1300 nm, Telesto II, Thorlabs, Bergkirchen, Germany). Between the light source and detector, we connected the intravascular imaging probe as the sample arm, and a reference arm consisting of a fiber patch cable and a movable mirror on a motorized linear stage (X-LSM, Zaber, Vancouver, Canada). We tested the capability of scanning with the 3D-printed needle beam endoscopic probe with two rotation mechanisms: we rotated using a counterrotation motor[23] and pulled back with a linear stage for the *ex vivo* human study, enabling the acquisition of a 3D data volume. For the *in vivo* intracoronary porcine study, we utilized a high-speed rotary joint (Princetel, Hamilton Township, New Jersey, United States) and a linear stage controlled by a MATLAB program (NinePoint Medical, Bedford, Massachusetts, United States).

2.4 Ex Vivo *Imaging of the Human Arteries*

The human study was approved by the Central Adelaide Local Health Network Human Research Ethics Committee (HREC15210). The arteries from patients undergoing clinically indicated carotid or femoral endarterectomy were dissected using the standard surgical technique. Instead of discarding the arteries as in the standard protocol, these specimens were collected and then scanned by our 3D-printed needle-beam endoscopic probes. After imaging, the sample was decalcified by 10% ethylenediaminetetraacetic acid for a week, embedded in paraffin, and sectioned for further histology analysis.

2.5 In Vivo *Intracoronary Imaging of Swine*

The porcine study was approved by the South Australian Health and Medical Research Institution animal ethics committee (SAM-21-011) and conducted according to the Australian code for the care and use of animals for scientific purposes (8th ed, 2013; updated 2021). Male Yorkshire swine (35 to 36 kg) were treated with streptozotocin (50 mg/kg on days 1 and 2 then 100 mg/kg on day 3) to induce diabetes, defined as a consistent blood glucose level >8.3 mmol/L. Starting at the time of diabetes induction, the animals were fed an atherogenic diet. Serum glucose was monitored serially, and insulin was administered to keep glucose levels <30 mmol/L and prevent ketoacidosis. Animal weights and blood glucose levels were monitored monthly. After feeding the animals for more than 3 months, the first intracoronary imaging procedures were conducted. Twenty-four hours prior to imaging, the swine were given a fentanyl patch as a pain killer. Prior to the procedure, meloxicam was given via intramuscular (IM) injection at the time of imaging to ensure full pain relief.

On the day of imaging, the animals were sedated with a mixture of xylazine and ketamine (IM injection) after which the animal was intubated and ventilated with oxygen (100% v/v). Anesthesia was maintained by isoflurane inhalation (4% to 5% for induction and 2% to 3% for maintenance) with constant oxygen ventilation (2 to 3 L/h). Access to the porcine coronary system was obtained percutaneously via a femoral artery. A standard 6-F coronary guiding catheter (AL2) was introduced via a 6-F sheath into one of the three main coronary arteries under X-ray and angiographic guidance. The 3D-printed needle-beam endoscopic probe was advanced into the coronary artery via the guiding catheter over a coronary angioplasty wire. Heparin, which has a half-life of ∼1 h, was administered during the imaging procedure to prevent thrombus formation on the device and wire. Imaging was performed by automated pullback under the injection of contrast agent flush rate of 4 mL/s. Following the imaging procedure, all catheters were removed, and the sheath was removed; hemostasis was obtained by manual pressure. Antibiotics were used as required under veterinary guidance.

The animals were closely monitored and continuously fed with an atherogenic diet for another 6 months after the first imaging procedure. The terminal imaging procedures were conducted similarly to the protocol described above via right femoral artery access. The 3D-printed needle-beam endoscopic probe was advanced into the same coronary arteries as imaged at the 3-month time point using X-ray angiography guidance, as outlined above. At the conclusion of the study, animals were euthanized, and their coronary arteries were processed for histology.

3 Results

3.1 Characterization of the Fabricated Needle-Beam Endoscopic Probe

To evaluate the resolutions (x- and y-axes) and DOF of the 3D-printed needle-beam probe, we characterized its spatial resolutions as a function of depth in both the x- and y-axes using an OCT resolution phantom [Fig. 2(a), APL-OP01, Arden Photonics, Solihull, United Kingdom]. Figures 2(b)–2(e) display the OCT images acquired by moving the resolution phantom along the x- and y-axes, where x is defined along the axis of the optical fiber, and y is perpendicular to this and to the direction of the light beam. As demonstrated in Figs. 2(b) and 2(d), a nearly astigmatism-free beam was achieved with the 3D-printed needle-beam probe inside the inner tube and a commercial intracoronary catheter sheath. To compare this with a more traditional optical design, we then placed a GRIN fiber probe[27] with both tubes at an equal distance to the resolution phantom. This design of GRIN fiber probe design is commonly used to make OCT endoscopes.[28] The resolution and DOF of the GRIN probe were observed to be inferior to that of the 3D-printed needle-beam probe [see Figs. 2(c) and 2(e)]. The 3D-printed probe can clearly resolve the bars 11 to 20 μm spacing [i.e., the $m = 2$ and $m = 3$ vertical lines in Figs. 2(b) and 2(d)] for more than 500 μm in depth, whereas the GRIN fiber probe was unable to resolve any bars between 11 and 20 μm spacing. To confirm the resolution test and further characterize the performance of the needle-beam probe, we performed a beam-profile measurement. As measuring the beam of the full micro-endoscope assembly with two layers of catheters in a water-like medium would be difficult to perform and prone to experimental inaccuracies, we adjusted the optical design to work in the air by making the TIR surface flat. Thus, the functionality of the micro-axicon lens can be singled out and characterized precisely in this way. As illustrated in Fig. S1 in the Supplementary Material, resolutions of less than 8 μm were measured with a DOF of nearly 800 μm.
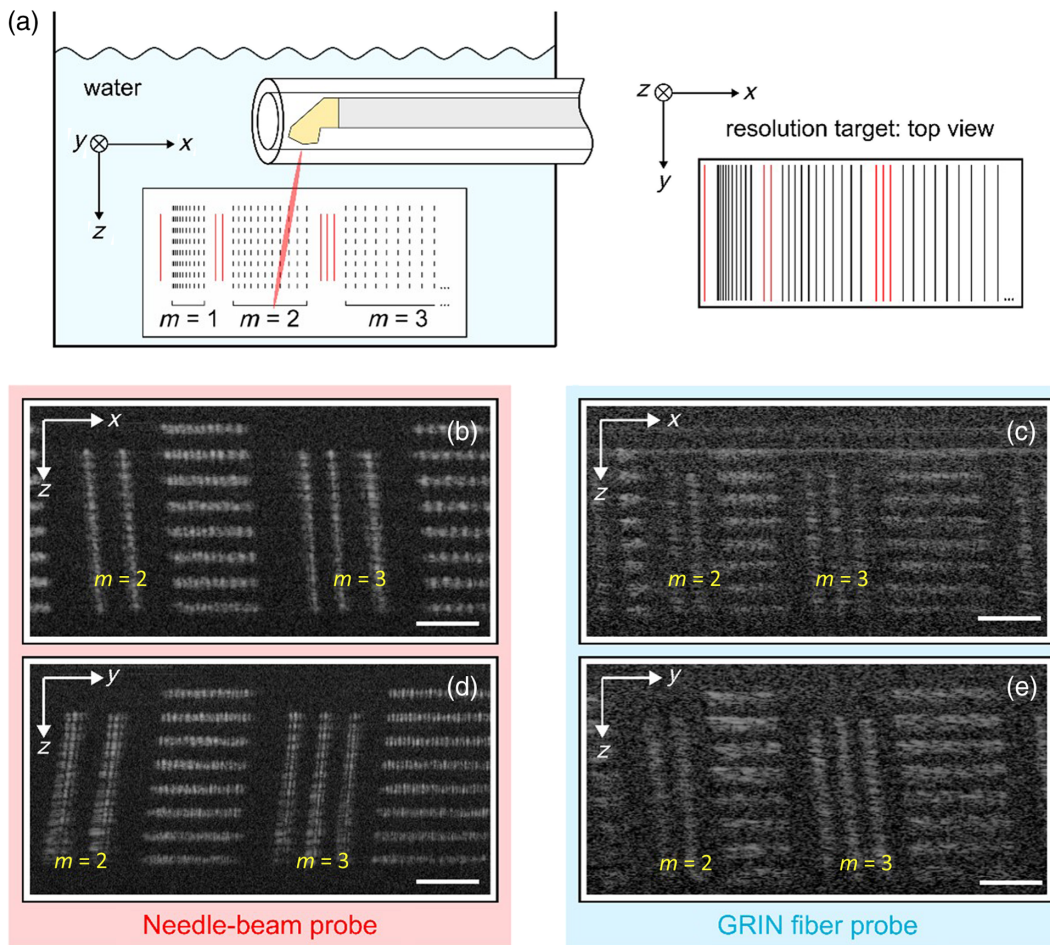
Fig. 2 Resolution characterization. (a) Sketch of the resolution measurement. A resolution target (APL-OP01, Arden Photonics, Solihull, United Kingdom) was pulled back relative to the 3D-printed needle-beam probe along the x axis and later along the y axis, resulting in two OCT scans—xz and yz, respectively. The lateral resolution pattern on the APL-OP01 target contains eight layers. The separation among each subsequent layer is 75 μm (physical distance), so the bottom layer is 525 μm from the top layer (physical distance). The purpose of the lateral resolution pattern is to measure the line spacing. Each line (n) is separated from the next line ($n + 1$) laterally by a distance of $11(m - 1) + n$, where m is the group number. (b) OCT image of the lateral resolution target obtained by the 3D-printed needle-beam probe along the x axis in Fig. 1(b). (c) OCT image of the lateral resolution target obtained by a conventional GRIN fiber probe along the x axis. (d) OCT image of the lateral resolution target obtained by the 3D-printed needle-beam probe along the y axis. (e) OCT image of the lateral resolution target obtained by a conventional GRIN fiber probe along the y axis. All images are obtained with the endoscopic probe placed inside the same inner tube, intracoronary catheter sheath and in water. The 3D-printed lens has a significantly more extended DOF than that of a GRIN fiber probe. Scale bars indicate optical distances, and the refractive index of the resolution validation phantom is 1.45. Scale bar: 250 μm.

Furthermore, we performed confocal measurements of our 3D-printed needle-beam lens to confirm that the shape deviations were not the limiting factor for the beam quality. We verify that the topographies of the axicon surface and the biconical TIR surface (Fig. S2 in the Supplementary Material) looked as expected and the peak-to-valley shape deviations for both surfaces were less than 1 μm, as is depicted in Fig. S3 in the Supplementary Material. By frequency-filtering the topographies, we extracted high spatial frequencies (higher than 0.125 $\mu\mathrm{m}^{-1}$) and obtained roughness of the axicon and TIR surface, which were Sq = 32.5 nm and Sq = 14.3 nm, respectively. The corresponding topographies are illustrated in Fig. S4 in the Supplementary Material.

## 3.2 Capability to Image Human Arteries with Advanced Plaques

We next imaged *ex vivo* human arteries to explore the improved imaging capability of the 3D-printed needle-beam probe when compared with a conventional OCT GRIN fiber probe. A schematic of such a GRIN probe is given in Fig. S5 in the Supplementary Material, and the comparisons of SNRs of the GRIN and 3D-printed needle-beam probes are presented in Figs. S6 and S7 in the Supplementary Material. Figure 3 presents the images obtained in a carotid plaque from a patient who had undergone a carotid endarterectomy after suffering

a stroke. Figures 3(a) and 3(b) and Video 1 are the 3D reconstruction of the plaque obtained using the 3D-printed needle-beam endoscopic probe. To ensure that the scans acquired with the 3D-printed and the GRIN fiber probes were colocated for comparison, we held the carotid plaque inside a tube to restrain its movement (Fig. S8 in the Supplementary Material). When imaged with the 3D-printed needle-beam probe, microstructures in the plaques were visible, as illustrated in Fig. 3(c), including acicular (cholesterol) clefts, a feature of high-risk atherosclerotic plaques. The standard GRIN fiber probe [Fig. 3(d)] was unable to resolve individual clefts. This correlates with our earlier measures of the OCT resolution phantom, as individual cholesterol clefts are typically ∼20 μm in size. The existence of cholesterol clefts identified by the 3D-printed probe [Fig. 3(c)] was validated by the hematoxylin and eosin (H&E) histology image [Figs. 3(e) and 3(h)]. During histological processing, the tube restricting tissue movement was removed to enable histological sectioning. As a result, the lumen of the carotid plaque

appeared larger in the histology image [Fig. 3(e)] than those in Figs. 3(c) and 3(d). Figures S9 and S10 in the Supplementary Material illustrate 3D reconstructions and OCT images of a necrotic core and a calcified plaque taken from additional human artery samples, respectively. The 3D-printed needle-beam images provide a clear visualization of the microstructure of the plaques, further validating the capability of the 3D-printed needle-beam probe to visualize near-cellular features (Video 2, MP4, 62.8 MB [URL: https://doi.org/10.1117/1.AP.7.2.026003.s2]).

3.3 Capability to Image Inside a Coronary Artery In Vivo

We performed two *in vivo* porcine experiments to assess the capabilities of the 3D-printed needle-beam probe. These experiments used a previously published porcine model of atherosclerosis,[29,30] in which a diabetic swine had been fed an
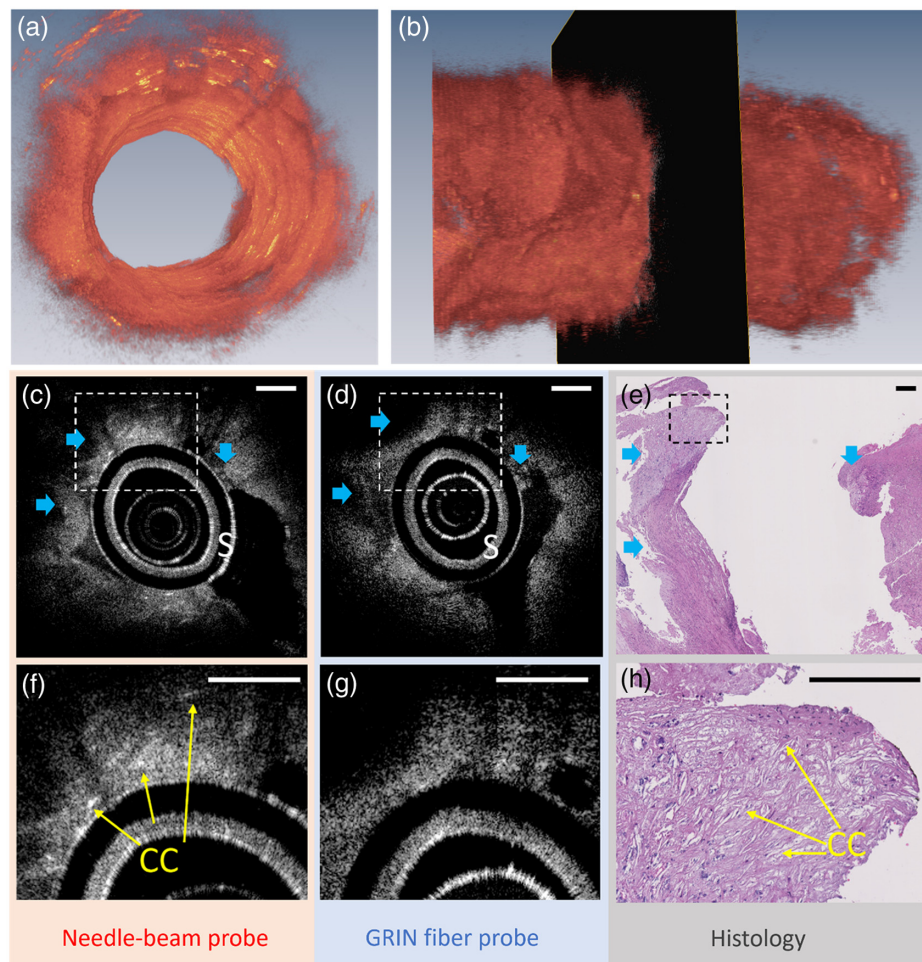
Fig. 3 *Ex vivo* comparison of 3D-printed needle-beam probe with conventional OCT probe imaging in a human carotid artery with advanced plaque. (a) and (b) 3D rendering of the artery created by 210 frames of OCT images obtained with a 3D-printed needle-beam endoscopic probe. (c) Representative OCT image obtained at the black box in (b) the 3D-printed needle-beam endoscopic probe. (d) Representative OCT image obtained at the same location by a GRIN fiber probe. (e) Corresponding H&E histology image. (f)–(h) Magnified views of the dashed line regions in panels (c)–(e). Blue arrows denote the landmark features used for matching needle-beam, GRIN, and histology images. CC, cholesterol clefts; S, sheaths. Scale bar: 250 μm (Video 1, MP4, 4.02 MB [URL: https://doi.org/10.1117/1.AP.7.2.026003.s1]).
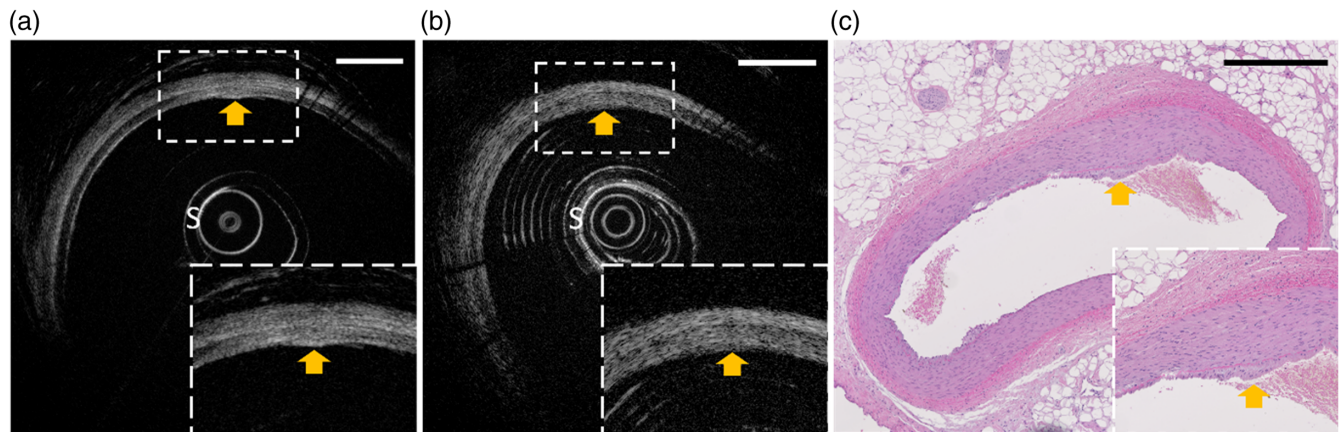
Fig. 4 *In vivo* imaging capability of 3D-printed needle-beam probe in comparison with a conventional GRIN fiber OCT probe. Images of a porcine circumflex coronary artery with early neointimal hyperplasia, highlighted by the orange arrows. (a) Image obtained with a 3D-printed needle-beam endoscopic probe. (b) Image obtained with a conventional GRIN fiber OCT probe. (c) Matching H&E histology image confirming the presence of neointimal hyperplasia (orange arrow). S, sheaths. Scale bar: 0.5 mm.

atherogenic diet for 11 months. In the first of these experiments, we conducted intracoronary imaging with both needle-beam and GRIN fiber probes. As demonstrated in the subimages of Fig. 4, this coronary artery began to develop an eccentric lesion of neointimal hyperplasia, labeled with an orange arrow at 12 o'clock in the figure. The 3D-printed needle-beam endoscopic probe showed clear differentiation of the neointimal hyperplasia [Fig. 4(a)]. In contrast, the conventional OCT GRIN fiber probe [Fig. 4(b)] showed poor differentiation of these layered structures and was unable to visualize the neointimal hyperplasia. The lower-quality GRIN images are representative of what has previously been reported in the literature.[31] The presence of neointimal hyperplasia was subsequently validated by H&E histology, as depicted in Fig. 4(c).

3.4 In Vivo *Intracoronary Imaging of Swine across Multiple Time Points*

In a second *in vivo* porcine study, we conducted serial imaging of the coronary arteries of a live pig. Images obtained in the anterior interventricular artery at 3 and 9 months after the commencement of the atherogenic diet are shown in Fig. 5. These time points allow an analysis of two stages of plaque development (early and advanced).[32,33]

The 3D-printed needle-beam probe was inserted percutaneously through the femoral artery of the swine [Fig. 5(a)]. Under X-ray and angiographic guidance [Fig. 5(b)], the probe was guided into the coronary arteries, which arise from the aorta and supply the heart with blood. Both the circumflex and anterior descending coronary arteries were safely imaged at 50 fps by the 3D-printed needle-beam probe. The swine successfully recovered from anesthesia after the imaging procedure. A representative image obtained with our 3D-printed needle-beam probe in the anterior interventricular artery at the 3-month time point is shown in Fig. 5(c). It highlights the three-layered arterial structure with intima [i.e., the label "I" in Fig. 5(c)], media [i.e., the label "M," by visualizing the internal elastic lamina (IEL) between the intima and the media in Fig. 5(c)], and adventitial [i.e., the label "A" in Fig. 5(c)]. The bright spot at 6 to 7 o'clock

of Fig. 5(c) (labeled with "G") is an artifact created by the coronary guide wire, which was used to advance and place the endoscopic probe in the coronary artery. There were no complications after the imaging procedure, and the swine continued the atherogenic diet for another 6 months before repeat surgery and imaging.

At the 9-month time point, the coronary arteries were successfully re-imaged using the 3D-printed needle-beam probe. As displayed in Figs. 5(d) and 5(e), we observed mild progression of the intimal thickening compared with the 3-month time point. In the images shown, intimal thickening can be appreciated at 9 to 12 o'clock (labeled "Plaque" to indicate the position of the atherosclerotic plaque). The presence of plaque was subsequently confirmed using colocated ionized calcium-binding adapter molecule 1 (Iba1)-stained histology [Fig. 5(e)], which was obtained by harvesting the coronaries after the swine were sacrificed following the 9-month time point *in vivo* imaging. The plaque was densely filled with macrophages, appearing in the OCT image as a homogeneous region of densely packed scatters with uniform speckles [9 to 12 o'clock in Fig. 5(d)]. This contrasts with the normal tissue structure at the 3-month time point, which appears to be more heterogeneous and displays a clear layered structure indicating different tissue types [9 to 12 o'clock in Fig. 5(c)]. Figure S11 in the Supplementary Material further illustrates the capability of a 3D-printed needle-beam probe to visualize near-cellular macrophage structure by contrasting a plaque in the circumflex coronary artery with the tissue layers delineated on the opposite side of the lumen, with a matching colocated H&E histology section.

4 Discussion and Conclusion

To the best of our knowledge, this paper presents the first report of a 3D-printed needle-beam endoscopic probe. This 3D-printed side-viewing freeform lens includes a micro-axicon lens to create a needle beam and a biconic surface to precompensate non-chromatic aberration in the system. The results established the ability of this probe to safely obtain OCT imaging with a resolution under 8 μm over a DOF of ∼800 μm in the torturous
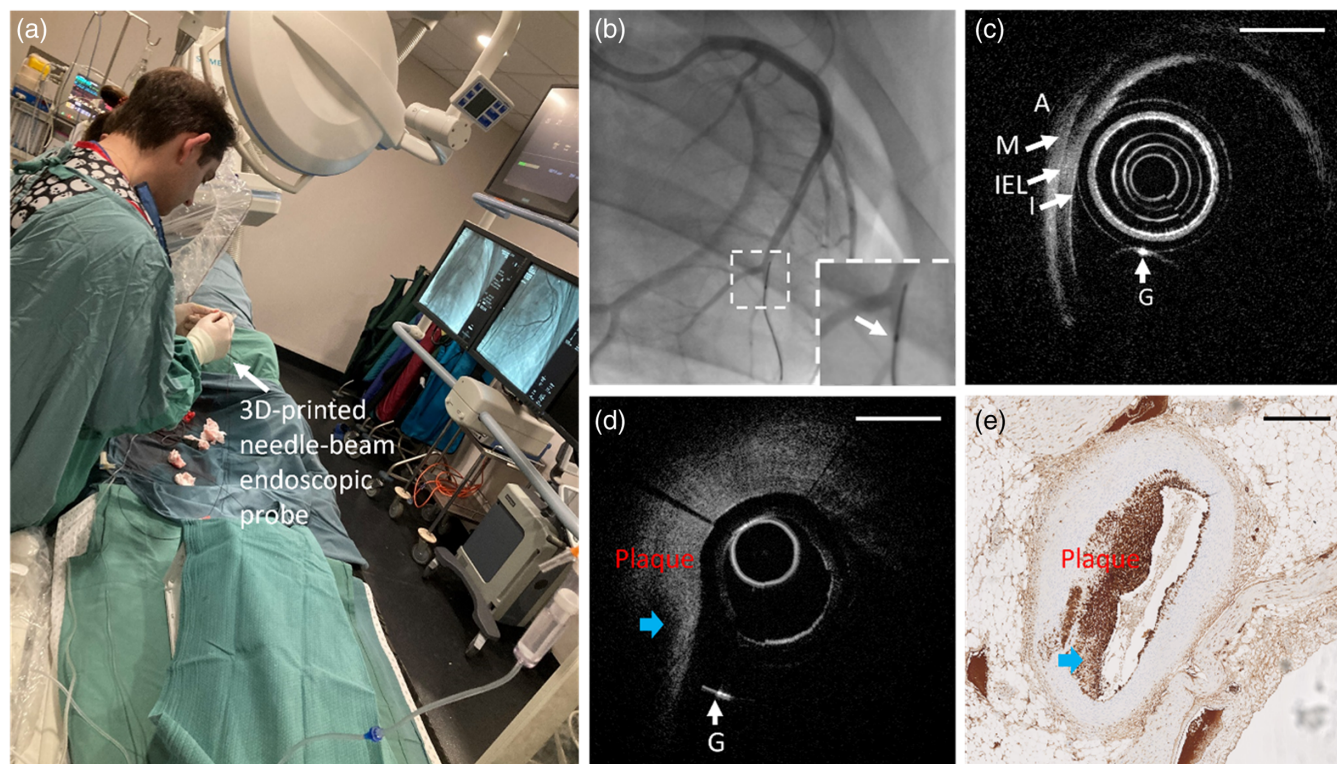
Fig. 5 Serial intracoronary imaging in a live swine with our 3D-printed needle-beam endoscopic probe. (a) Cardiac catheterization laboratory setup for the intracoronary imaging procedure, where an interventional cardiologist inserts the 3D-printed needle-beam endoscopic probe into the coronary artery of the anesthetized swine via right femoral artery access. (b) X-ray angiography image showing the placement of the 3D-printed endoscopic probe in the anterior interventricular artery. Inset: magnified version with an arrow denotes the radiopaque marker at the tip of the 3D-printed needle-beam endoscopic probe. (c) Representative OCT image obtained in the anterior interventricular artery at the 3-month time point. (d) Representative OCT image obtained in the anterior interventricular artery at the 9-month time point. (e) Matching ionized calcium-binding adapter molecule 1 (Iba1)-stained histology image of panel (d). Blue arrows pointing to the necrotic region of this plaque. I, intima; IEL, internal elastic lamina; A, adventitia; G, guidewire. Scale bar: 0.5 mm.

arterial systems and coronary arteries in living animals at multiple time points. This work addresses one of the major limiting features of clinical OCT. The micro-optic design can be tailored for different probes, catheter sheaths, and applications to achieve optimized beam quality and image performance.

Realizing compact fiber-based endoscopes with large DOF and high resolution has previously been technically challenging. Two-photon polymerization 3D printing enables the implementation of compact but complex optics directly on a fiber tip. Such fibers with 3D-printed micro-optics can be used in OCT-endoscopy applications and may help overcome the current limitations of small optics. The choice of scanning beam shape is a crucial question when designing such micro-optics. As we aim for a large DOF while preserving high resolution, i.e., narrow width of the beam along the axis, needle beams created by axicon-like lenses may provide a solution. The resulting needle-like focal shape, extended along its propagation axis, is suited for achieving the desired characteristics of the beam while preserving the compact size of the 3D-printed lens.

In our application, we use a 3D-printed micro-axicon lens to create a needle beam over the region of interest along the optical axis, with a typical artery diameter of 2 to 3 mm. However, the diameter of an artery varies significantly from its proximal to distal end (from ∼20 mm to a few hundreds of micrometers). Accordingly, the images obtained by our 3D-printed micro-axicon lens were well suited for a lumen with a small diameter (e.g., Fig. 3) but did demonstrate the lens's limitation when the diameter of the artery lumen was larger and the plaque further from the axicon lens [e.g., Fig. 5(d)]. Similar to Gaussian beams, the resolution and DOF of the needle beam are dependent on the geometric parameters of the lens, including its diameter. Therefore, restricting the lens diameter to less than 300 μm while achieving high resolution over a DOF of over 1 mm is still a challenging task.

The two-photon polymerization 3D-printing technique, as demonstrated here, is not only limited to create a needle-beam via an axicon lens but also allows the fabrication of other lenses/masks/filters[5,6,7,9,16–19] for beam-shaping/tailoring in various imaging modalities. This technique holds great hope to make beam tailoring in endoscopic probes more precise. Miniaturized endoscopic probes are widely needed for imaging small luminal or delicate organs (e.g., small airways and bile ducts).[34,35] However, current fabrication methods limit their performance in terms of resolution, depth of focus, and multimodal imaging capability

and, thus, restrict their applications.[28] Our versatile technique can find broad applications in other organs and diseases, although this work was strategically focused on showcasing the efficacy in cardiology.

Disclosures

Code and Data Availability

The data that support the findings of this study are available from the corresponding author upon reasonable request.

Acknowledgments

References

1. B. E. Bouma et al., "Intravascular optical coherence tomography [Invited]," *Biomed. Opt. Express* **8**(5), 2660–2686 (2017).
2. R. Puri, M. I. Worthley, and S. J. Nicholls, "Intravascular imaging of vulnerable coronary plaque: current and future concepts," *Nat. Rev. Cardiol.* **8**(3), 131 (2011).
3. J. Li et al., "Ultrathin monolithic 3D printed optical coherence tomography endoscope for preclinical and clinical use," *Light: Sci. Appl.* **9**(1), 124 (2020).
4. H. Pahlevaninezhad et al., "Nano-optic endoscope for high-resolution optical coherence tomography in vivo," *Nat. Photonics* **12**(9), 540–547 (2018).
5. L. Liu et al., "Imaging the subcellular structure of human coronary atherosclerosis using micro–optical coherence tomography," *Nat. Medicine* **17**(8), 1010–1014 (2011).
6. B. Yin et al., "3D cellular-resolution imaging in arteries using few-mode interferometry," *Light: Sci. Appl.* **8**(1), 104 (2019).
7. J. Zhao et al., "Flexible method for generating needle-shaped beams and its application in optical coherence tomography," *Optica* **9**(8), 859–867 (2022).
8. J. Kang et al., "Pencil-beam scanning catheter for intracoronary optical coherence tomography," *Opto-Electron. Adv.* **5**(3), 200050 (2022).
9. T. Vettenburg et al., "Light-sheet microscopy using an Airy beam," *Nat. Methods* **11**(5), 541–544 (2014).
10. S. Takanezawa, T. Saitou, and T. Imamura, "Wide field light-sheet microscopy with lens-axicon controlled two-photon Bessel beam illumination," *Nat. Commun.* **12**(1), 2979 (2021).
11. B. Chen et al., "Rapid volumetric imaging with Bessel-beam three-photon microscopy," *Biomed. Opt. Express* **9**(4), 1992–2000 (2018).
12. J. Wu, N. Ji, and K. K. Tsia, "Speed scaling in multiphoton fluorescence microscopy," *Nat. Photonics* **15**(11), 800–812 (2021).
13. B. Jiang, X. Yang, and Q. Luo, "Reflection-mode Bessel-beam photoacoustic microscopy for *in vivo* imaging of cerebral capillaries," *Opt. Express* **24**(18), 20167–20176 (2016).
14. J. Shi et al., "Bessel-beam Grueneisen relaxation photoacoustic microscopy with extended depth of field," *J. Biomed. Opt.* **20**(11), 116002 (2015).
15. W. Wang et al., "Miniature all-fiber axicon probe with extended Bessel focus for optical coherence tomography," *Opt. Express* **27**(2), 358–366 (2019).
16. J. Kim et al., "Endoscopic micro-optical coherence tomography with extended depth of focus using a binary phase spatial filter," *Opt. Lett.* **42**(3), 379–382 (2017).
17. D. Lorenser, X. Yang, and D. D. Sampson, "Ultrathin fiber probes with extended depth of focus for optical coherence tomography," *Opt. Lett.* **37**(10), 1616–1618 (2012).
18. D. Cui et al., "Flexible, high-resolution micro-optical coherence tomography endobronchial probe toward *in vivo* imaging of cilia," *Opt. Lett.* **42**(4), 867–870 (2017).
19. B. Yin et al., "Extended depth of focus for coherence-based cellular imaging," *Optica* **4**(8), 959–965 (2017).
20. Z. Yang et al., "A compact Airy beam light sheet microscope with a tilted cylindrical lens," *Biomed. Opt. Express* **5**(10), 3434–3442 (2014).
21. W. D. Sacher et al., "Implantable photonic neural probes for light-sheet fluorescence brain imaging," *Neurophotonics* **8**(2), 025003 (2021).
22. S. Turtaev et al., "High-fidelity multimode fibre-based endoscopy for deep brain in vivo imaging," *Light: Sci. Appl.* **7**(1), 92 (2018).
23. J. Li et al., "3D-printed micro lens-in-lens for in vivo multimodal microendoscopy," *Small* **18**(17), 2107032 (2022).
24. J. Li et al., "Integrated IVUS-OCT for real-time imaging of coronary atherosclerosis," *JACC Cardiovasc. Imaging* **7**(1), 101–103 (2014).
25. F. Lux et al., "3D nanoprinted catadioptric fiber sensor for dual-axis distance measurement during vitrectomy," *Appli. Opt.* **63**(11), 2806–2814 (2024).
26. J. Weinacker et al., "On iterative pre-compensation of 3D laser-printed micro-optical components using confocal-optical microscopy," *Adv. Funct. Mater.* **34**(12), 2309356 (2024).

27. J. Walther et al., "A handheld fiber-optic probe to enable optical coherence tomography of oral soft tissue," *IEEE Trans. Biomed. Eng.* **69**(7), 2276–2282 (2022).

28. M. J. Gora et al., "Endoscopic optical coherence tomography: technologies and clinical applications [Invited]," *Biomed. Opt. Express* **8**(5), 2405–2444 (2017).

29. D. Hamamdzic and R. L. Wilensky, "Porcine models of accelerated coronary atherosclerosis: role of diabetes mellitus and hypercholesterolemia," *J. Diabetes Res.* **2013**, 761415 (2013).

30. S. C. Yiannis et al., "Prediction of the localization of high-risk coronary atherosclerotic plaques on the basis of low endothelial shear stress," *Circulation* **117**(8), 993–1002 (2008).

31. Jiechen Yin et al., "Integrated intravascular optical coherence tomography ultrasound imaging system," *J. Biomed. Opt.* **15**(1), 010512 (2010).

32. C. K. Konstantinos et al., "Natural history of experimental coronary atherosclerosis and vascular remodeling in relation to endothelial shear stress," *Circulation* **121**(19), 2092–2101 (2010).

33. R. G. Gerrity et al., "Diabetes-induced accelerated atherosclerosis in swine," *Diabetes* **50**(7), 1654–1665 (2001).

34. J. M. Poneros et al., "Optical coherence tomography of the biliary tree during ERCP," *Gastrointest. Endosc.* **55**(1), 84–88 (2002).

35. Y. Chen et al., "Validation of human small airway measurements using endobronchial optical coherence tomography," *Respir. Med.* **109**(11), 1446–1453 (2015).

36. M. Schmid et al., "Three-dimensional direct laser written achromatic axicons and multi-component microlenses," *Opt. Lett.* **43**(23), 5837–5840 (2018).

37. M. Schmid et al., "3D printed hybrid refractive/diffractive achromat and apochromat for the visible wavelength range," *Opt. Lett.* **46**(10), 2485–2488 (2021).

38. A. Agrawal et al., "Methods to assess sensitivity of optical coherence tomography systems," *Biomed. Opt. Express* **8**(2), 902–917 (2017).

Pavel Ruchka received his MS degree in photonic engineering from University of Stuttgart (Germany) in 2021. He is a final-year doctoral researcher at the University of Stuttgart, 4th Physics Institute (group of Prof. Dr. Harald Giessen) and a part of the interdisciplinary research training group (RTG 2642) for photonic quantum engineers, funded by German Research Council (DFG). His research activities are focused on three-dimensional (3D) printing and its applications to quantum technologies and medical optics.

Harald Giessen is head of the 4th Physics Institute and the Stuttgart Research Center of Photonics Engineering (SCoPE) at University of Stuttgart. He obtained his MSc and PhD in optical sciences from the University of Arizona, followed by a postdoc at the Max Planck Institute in Stuttgart and an assistant professorship at University of Marburg and an associate professorship at University of Bonn. His research focus is ultrafast nanooptics, plasmonics, and 3D-printed microoptics.

Jiawen Li is an associate professor at the School of Electrical and Mechanical Engineering and serves as the deputy director of the Institute for Photonics and Advanced Sensing at the University of Adelaide. She received her BS degree in optical engineering from Zhejiang University in 2010 and her PhD in biomedical engineering from the University of California, Irvine, in 2015. Her research focuses on multimodal imaging, fiber-optic sensing, optical coherence tomography, and 3D-printed devices.

Biographies of the other authors are not available.